

## Detection of long-range orbital-Hall torques


Arnab Bose <sup>1,\*</sup> Fabian Kammerbauer <sup>1</sup> Rahul Gupta <sup>1</sup> Dongwook Go <sup>1,2</sup> Yuriy Mokrousov,<sup>1,2</sup>  
Gerhard Jakob <sup>1,3</sup> and Mathias Kläui <sup>1,3,4,†</sup>

<sup>1</sup>*Institute of Physics, Johannes Gutenberg University Mainz, Staudingerweg 7, 55128 Mainz, Germany*

<sup>2</sup>*Peter Grünberg Institut and Institute for Advanced Simulation, Forschungszentrum Jülich and JARA, 52425 Jülich, Germany*

<sup>3</sup>*Graduate School of Excellence Materials Science in Mainz, 55128 Mainz, Germany*

<sup>4</sup>*Center for Quantum Spintronics, Department of Physics, Norwegian University of Science and Technology, NO-7491 Trondheim, Norway*

 (Received 4 August 2022; revised 31 March 2023; accepted 31 March 2023; published 19 April 2023)

We report and quantify a large orbital-Hall torque generated by Nb and Ru, which we identify from the strong dependence of torques on the ferromagnets. This is manifested as strong enhancement in the dampinglike torques measured in Nb (or Ru)/Ni bilayers as compared to Nb (or Ru)/FeCoB bilayers including the sign reversal in the case of Nb/(Ni or FeCoB) samples. We experimentally observe a striking enhancement of the measured torques with the increase of ferromagnetic Ni thickness which is markedly different from the regular spin-transfer torque; this could be a unique signature of long-range action of the orbital-Hall torques.

DOI: [10.1103/PhysRevB.107.134423](https://doi.org/10.1103/PhysRevB.107.134423)

### I. INTRODUCTION

The nonequilibrium flow of angular momentum has been one of the key aspects of condensed matter physics, as it plays a major role in modern solid-state magnetic devices [1,2]. Nature provides two different types of intrinsic angular momenta in a material that can be relatively easily accessible for applications, which are orbital-angular momentum and spin-angular momentum. In the past decade, the main focus of spintronics has been to inject spin angular momentum into a magnet for nonvolatile memory applications [1,2], which was triggered by the discovery of the spin-Hall effect (SHE) [3], a mechanism that generates a transverse spin current ( $J_{SH}$ ) which can interact with the magnet directly via a spin-transfer torque (STT) [1]. However, this scheme of strong  $J_{SH}$  generation is mostly limited to certain materials due to the requirement of large spin-orbit coupling (SOC) such as Pt, W, etc. [1]. Recent theoretical works have predicted the generation of large orbital-Hall current ( $J_{OH}$ ) from the orbital-Hall effect (OHE), not relying on the SOC of the nonmagnetic material (NM) [4–13]. However,  $J_{OH}$  remains challenging for an unambiguous experimental detection [14] since  $J_{OH}$  does not interact directly with the magnetization of commonly studied ferromagnets (FMs) [7–9], unlike  $J_{SH}$  which generates STT in a magnetic layer that is largely independent of the FM [1]. So far, the orbital-Hall torques (OHTs) have often been studied in systems with naturally grown oxides such as  $\text{CuO}_x$  and  $\text{AlO}_x$  as the nonmagnetic layer [15–19], and these oxide layers are often not well controlled, making it difficult to compare the results with the theoretical calculations. Therefore, it is of prime interest to study this effect in clean and well-defined elements for a direct and unambiguous comparison.

### II. BACKGROUND AND THEORY

While the spin-orbit torques (SOTs) are essential ingredients for memory applications there have been strong disagreements in the predicted and experimentally measured torques [1] in some systems including the sign reversal [20–23], suggesting an important piece of physics is still missing. By the SHE mechanism, longitudinal electric current ( $J_C$ ) flowing along the  $x$  direction in the heavy metals (HMs) generates a flow of spins perpendicular to it (along the  $z$  axis, sample growth direction) while the spins are polarized along  $y$  [Fig. 1(a)]. Similarly, in certain nonmagnets it has been predicted to have the flow of transverse orbital angular momentum (along the  $z$  axis) from the  $J_C$  (along the  $x$  axis) with the orbital quantization axis being along  $y$  [5] [Fig. 1(a); the orbital moment is normal to the drawn circles]. This is referred to as orbital-Hall current ( $J_{OH}$ ). Its advantage is that large values of  $J_{OH}$  can be found in abundant materials uncorrelated to the SOC that could be used for practical applications.

The actions of  $J_{SH}$  and  $J_{OH}$  are distinctly different on the FM.  $J_{SH}$  can directly interact with the static magnetization of the adjacent FM and thereby produces the dampinglike torque (DLT) efficiency,  $\xi_{DL} = T\theta_{SH}$  (where  $\theta_{SH}$  is the internal spin-Hall angle) nearly independent of the FM in the commonly studied HM/FM bilayers due to the comparable magnitude of the spin transparency ( $T$ ) [1]. On the other hand,  $J_{OH}$  does not directly interact with the FM. However, it was recently predicted that the injected  $J_{OH}$  can be converted into the spin current ( $J_{OH \rightarrow S}$ ) inside some of the FMs using the SOC of the FM, having nonzero orbital quenching as schematically shown in Fig. 1(b) and hence  $J_{OH \rightarrow S}$  would produce a torque on the FM, referred to as orbital-Hall torque (OHT) [7–9]. Ni is predicted to be very efficient for OHT while Fe is quite inefficient, suggesting a strong ferromagnet dependence that has been recently predicted [7–9], reported in some of the experimental works [21,23–27] and also corroborated in this work by comparing NM/Ni and NM/ $\text{Fe}_{60}\text{Co}_{20}\text{B}_{20}$  bilayers.

\*abose@uni-mainz.de

†klaui@uni-mainz.de

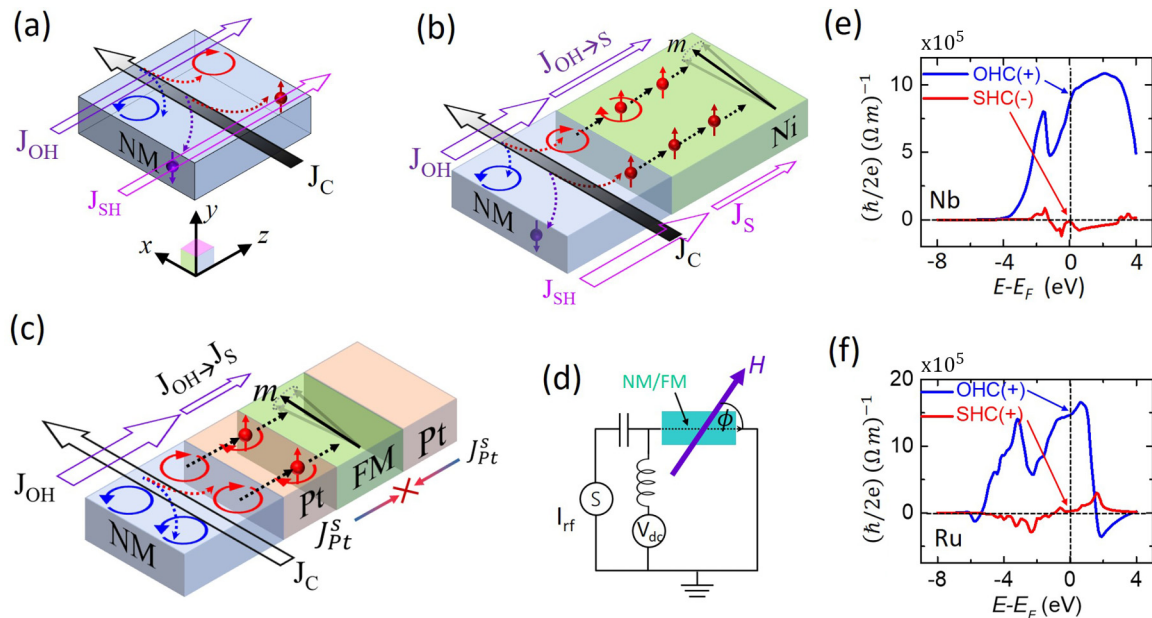


FIG. 1. (a) Schematics of the generation of  $J_{OH}$  from the OHE and  $J_{SH}$  from the SHE driven by  $J_C$  in NM. (b) Two different components of spin currents responsible for the SOT in the magnet: (1)  $J_S$ , the fraction of  $J_{SH}$  injected into the FM and (2)  $J_{OH \rightarrow S}$ , the converted spin current inside the FM from the generated  $J_{OH}$ . (c) Implementation of a NM/Pt/FM/Pt heterostructure. Externally injected  $J_{OH}$  from the NM (low SOC) is converted into  $J_{OH \rightarrow S}$  using the SOC of Pt that further produces a torque on FM.  $J_{SH}$  produced by both the Pt layers nearly cancel each other. (d) Schematic representation of the experimental setup. Calculated orbital-Hall conductivity (OHC) and spin-Hall conductivity (SHC) of Nb (e) and Ru (f) by DFT. The OHC is large and positive for both Nb and Ru at the Fermi level. The SHC is very small for both and negative for Nb (e) and positive for Ru (f).

Another key difference between  $J_{OH}$  and  $J_{SH}$  could be the length scale of the angular momenta (spin or/and orbital) transport inside the FM as pointed out in Ref. [9]. For example, the transverse component of the spins is absorbed within the first few monolayers of the FM [1,28,29], producing an interfacial torque which then spreads to the entire volume of the magnet. Therefore, the net spin-transfer torque (STT) is inversely proportional to the thickness of the magnet ( $t_{FM}$ ) and hence the  $\xi_{DL}$  should ideally be independent of  $t_{FM}$  as it is derived by dividing the net measured torque with the total magnetic volume per unit current density. However, Ref. [9] points out a different behavior that may occur in some cases for injected  $J_{OH}$  inside a FM with large SOC and small orbital quenching effects in which the  $J_{OH}$  can be transmitted over a long range inside the FM before it is fully converted into the spin current ( $J_{OH \rightarrow S}$ ) and hence is expected to result in a long-range torque effect [9]. This basically implies that the dampinglike torque efficiency driven by  $J_{OH \rightarrow S}$  within the FM will increase with  $t_{FM}$  and then tend to saturate. This can be phenomenologically expressed by the following equation:

$$\xi_{net} = \xi_{SH} + \xi_{OH}[1 - \text{sech}(t_{FM}/\lambda_{FM})], \quad (1)$$

where  $\xi_{SH}$  represents the conventional DLT as observed in the standard HM/FM bilayers in the absence of  $J_{OH}$ .  $\xi_{OH}$  represents the DLT due to the  $J_{OH \rightarrow S}$  which is strongly FM dependent [7–9]. The term  $[1 - \text{sech}(t_{FM}/\lambda_{FM})]$  suggests the long-range action of the torques while  $\lambda_{FM}$  sets the characteristic length scale that uniquely distinguishes OHT from the regular SHT. In this experimental work, we not only show a strong FM dependence, but also we report robust experimental

evidence of such long-range torques by systematically varying the thickness of the magnet (Ni) which has rarely been reported in previously studied systems [15,18,23–25,30]. We find that  $\lambda_{FM}$  of our ferromagnet, Ni, is approximately 2.5 nm suggesting that it takes 8–10 nm Ni thickness to get the full strength of the torques, nearly an order of magnitude larger than the length scale of the conventional SHT [28,29].

While the long-range torque is the primary focus of this work, we have also explored the  $J_{OH \rightarrow S}$  using the SOC of a HM (Pt in this case) rather than relying on the SOC of the FM by judiciously designing the stack: NM/Pt( $t$ )/FM/Pt( $t$ )/cap [Fig. 1(c)]. Our proposed device design eliminates the contribution from the regular SHE due to the symmetric placement of Pt on both sides of the FM which was also not considered in the previous reports [14,15,23–25] and thus our work presents a more comprehensive understanding of the fundamental interplay of  $J_{OH}$  and  $J_{SH}$  in spin-orbit coupled systems.

### III. SAMPLE PREPARATION

We study NM, Nb, and Ru as the source of  $J_{OH}$  as they are predicted to possess a large orbital-Hall conductivity (OHC) and negligible spin-Hall conductivity (SHC) by density functional theory (DFT) [Figs. 1(e) and 1(f)] that allows for a clean experimental detection of OHE [4,6,10]. Details of the DFT calculations can be found in the Supplemental Material [31]; also see Refs. [32–36] therein. Four different sets of samples are prepared on a highly resistive Si/SiO<sub>2</sub> wafer by the sputtering technique, set 1: Ru (or Nb)/Ni/cap; set 2: Ru (or Nb)/Fe<sub>60</sub>Co<sub>20</sub>B/cap; set 3: Ru (or Nb)/Pt( $t_{Pt}$ )/Fe<sub>60</sub>Co<sub>20</sub>B (or Ni<sub>81</sub>Fe<sub>19</sub>)/Pt( $t_{Pt}$ )/cap; set 4: Ru

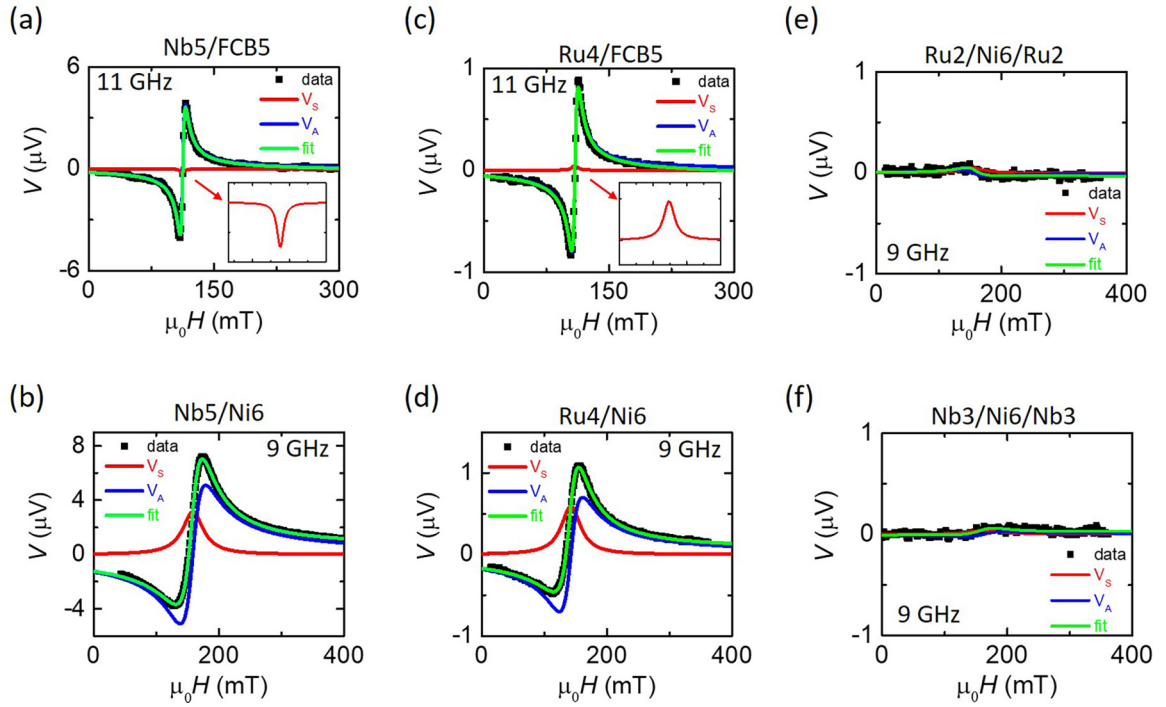


FIG. 2. Experimentally measured STFMR data in Nb (5 nm)/Fe<sub>60</sub>Co<sub>20</sub>B<sub>20</sub>(FCB) (5 nm) (a), Nb (5 nm)/Ni (6 nm) (b), Ru (4 nm)/FCB (5 nm) (c), Ru (4 nm)/Ni (6 nm) (d), Ru (2 nm)/Ni (6 nm)/Ru (2 nm) (e), and Nb (3 nm)/Ni (6 nm)/Nb (3 nm) (f). Black points are the experimental data which are fit to the green curve that is the sum of  $V_S$  (red curve),  $V_A$  (blue curve), and a constant dc offset.

(or Nb)/Ni/Ru (or Nb)/cap. The thickness of Ru and Nb is 4 and 5 nm, respectively. The thickness of Ni was varied from 4 to 12 nm. The thickness of Fe<sub>60</sub>Co<sub>20</sub>B<sub>20</sub> (FCB) and Ni<sub>81</sub>Fe<sub>19</sub> (Py) was varied from 4 to 6 nm. More details about the sample preparation can be found in the Supplemental Material [31].

#### IV. EXPERIMENTAL PROCEDURE

We performed spin-torque ferromagnetic resonance (STFMR) [37–39] to quantify the SOT. A radio frequency (rf) ( $f_0 = 7 - 12$  GHz) current is passed through the device and a dc voltage is measured while sweeping an in-plane external magnetic field ( $H$ ) at an angle  $\phi$  with respect to  $J_C$  as shown in Fig. 1(d). The magnet responds to the radio frequency Oersted field ( $H_{Oe}$ ) and the spin current ( $J_S$ ) produced by the adjacent layers and oscillates. A homodyne mixture of the oscillatory magnetoresistance due to anisotropic magnetoresistance (AMR) and oscillatory  $J_C$  produces a dc voltage [37–39] that is a superposition of symmetric ( $V_S = S[\frac{\Delta^2}{(H-H_0)^2 + \Delta^2}]$ ) and antisymmetric ( $V_A = A[\frac{(H-H_0)\Delta}{(H-H_0)^2 + \Delta^2}]$ ) Lorentzian lines.  $\Delta$  is the magnetic linewidth;  $H_0$  is the resonant field;  $S$  and  $A$  arise from the in-plane and out of plane torques, respectively. Unlike in single crystal materials, here we do not expect any extraordinary torques [40] as the sputtered films are typically polycrystalline. Hence the dominant origin of  $S$  is the in-plane damping-like torque (ipDLT) generated from the injected  $J_S$  into the FM whereas  $A$  originates from the out of plane field-like torques (opFLT) generated by the  $H_{Oe}$  and interfacial spin-orbit fields [39,41]. The efficiency of STFMR

[39] can be defined as

$$\xi_{\text{FMR}} = \frac{S}{A} \frac{e\mu_0 M_S t_{\text{NM}} t_{\text{FM}}}{\hbar} \sqrt{1 + \left(\frac{M_{\text{eff}}}{H_0}\right)^2}, \quad (2)$$

where  $\mu_0$  is the permeability;  $t_{\text{NM}}$  is the thickness of the NM;  $M_S$  and  $M_{\text{eff}}$  are the saturation magnetization and out of plane demagnetization field of the ferromagnet as determined by SQUID magnetometry and using Kittel's equation [37] (see Supplemental Material [31] for a detailed experimental technique). In the absence of interfacial spin-orbit fields (meaning  $H_{Oe}$  is the dominant source of opFLT)  $\xi_{\text{FMR}}$  becomes the measure of the DLT efficiency per unit current density,  $\xi_{\text{DL},j}$  [37,39]. DLT efficiency per unit longitudinal field (equivalent to the effective spin-torque conductivity) can be calculated as  $\xi_{\text{DL},E} = \xi_{\text{DL},j}/\rho_{xx}$  where  $\rho_{xx}$  is the longitudinal resistivity of the nonmagnet.  $\rho_{xx}$  of Nb (5 nm) and Ru (4 nm) are 41 and 27.3  $\mu\Omega$  cm, respectively, as calculated from a four-probe measurement technique.

#### V. EXPERIMENTAL RESULTS AND DISCUSSION

##### A. Strong ferromagnet dependence of the torques

Figures 2(a)–2(d) show the STFMR voltage spectra as a function of the external field ( $H$ ) sweep for Nb and Ru with the FM as FCB and Ni. Figures 2(a) and 2(c) show a small  $V_S$  signal (red curves) estimating a negligible DLT ( $|\xi_{\text{DL}}| \approx 0.001$ ) produced by both Nb and Ru. From the sign of  $V_S$  [zoomed-in inset of Figs. 2(a) and 2(c)], we confirm that Nb exhibits a negative sign of SHE (same sign as W [42,43]) and Ru exhibits a positive sign (same sign as Pt

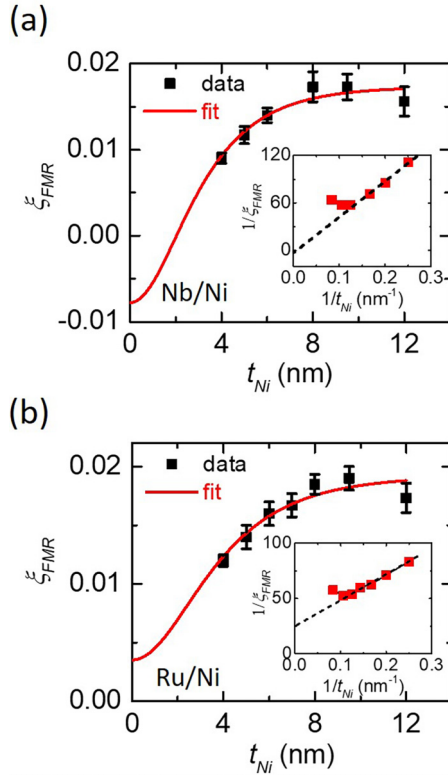


FIG. 3.  $\xi_{\text{FMR}}$  as a function of the thickness of Ni ( $t_{\text{Ni}}$ ) in Nb/Ni (a) and Ru/Ni (b) bilayers. The inset shows a plot of  $1/\xi_{\text{FMR}}$  against  $1/t_{\text{Ni}}$ . The red continuous line is the fit using Eq. (1).

[37,43]) but much smaller in magnitude, which is consistent with theoretical predictions [4,10] [Figs. 1(e) and 1(f)]. When the Ni is used as a FM, we find a dramatic increase of  $V_S$  for both Nb [Fig. 2(b)] and Ru [Fig. 2(d)] indicating a large DLT with positive sign for both cases that cannot be explained by the SHE. The enhanced DLT (for both Ru and Nb) including the sign change in  $V_S$  (for Nb) is consistent with Eq. (1) suggesting a large  $J_{\text{OH}}$  generated by the NM which is manifested as the OHT using Ni as a ferromagnetic detector while dominating over the SHT. Figures 2(e) and 2(f) show the negligible results when Ni is sandwiched between the symmetric layers (Ru/Ni/Ru and Nb/Ni/Nb samples). The measurements show that the self-induced torques, resonant heating, and other thermal artifacts are negligible [44]. Our data cannot be explained by the “self-induced torques” as that would lead to the opposite sign of the DLT as we observe for NM/Ni bilayers considering the sign of the SHE of Ni [45].

### B. Ferromagnet thickness dependence of the torques

Figure 3 shows the variations of  $\xi_{\text{FMR}}$  as a function of Ni thickness ( $t_{\text{Ni}}$ ) for both Nb [Fig. 3(a)] and Ru [Fig. 3(b)], showing robust experimental evidence of long-range torques, which can be well described by Eq. (1). Since the strong ferromagnet dependence in Nb(Ru)/Ni and Nb(Rb)/FCB as presented in Fig. 2 is consistent with the theory of orbital-Hall torques (OHTs) and is also consistent with the experimental

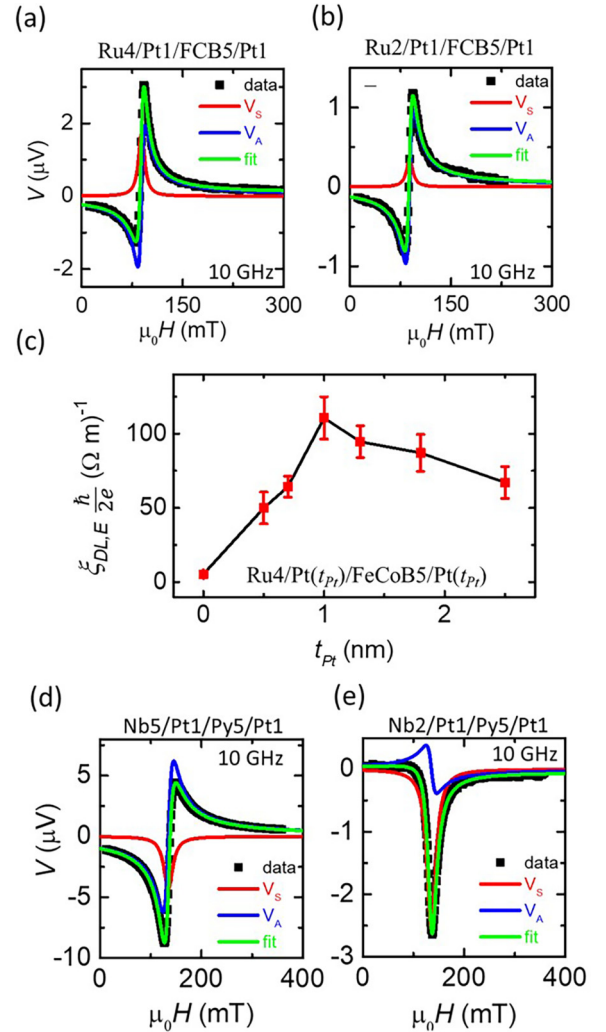


FIG. 4. Experimentally measured STFMR data in Ru/Pt/FCB/Pt for Ru thickness 4 nm (a) and 2 nm (b). (c) The dependence of the DLT efficiency per unit field ( $\xi_{\text{DL},E}$ ) as function of Pt thickness ( $t_{\text{Pt}}$ ) in symmetric Ru/Pt( $t_{\text{Pt}}$ )/FCB/Pt( $t_{\text{Pt}}$ ) heterostructures. Experimentally measured STFMR data in Nb/Pt/Py/Pt for Ru thickness 4 nm (d) and 2 nm (e).

reports of previous works [21,23–27], it is possible to attribute the variation of  $\xi_{\text{FMR}}$  with  $t_{\text{Ni}}$  (Fig. 3) to the combination of SHT and OHT as presented in Eq. (1). However, a detailed theoretical analysis is needed considering the actual electronic and band structures and interfacial hybridization between the thin-film nonmagnet (Ru or Nb) and ferromagnet (Ni), to fully understand this unusual behavior of the damping-like torques as shown in Fig. 3. At present, by fitting the experimental data with Eq. (1), we can quantify the possible contributions of SHE and OHE. The SHE contribution ( $\xi_{\text{SH}}$ ) is estimated to be small for both Nb ( $\xi_{\text{SH}} \approx -0.007$ ) and Ru ( $\xi_{\text{SH}} \approx +0.003$ ), which is qualitatively consistent with Figs. 2(a) and 2(c) and DFT calculations [Figs. 1(e) and 1(f)] [4,10]. The estimated OHT efficiencies per unit current ( $\xi_{\text{OH},j}$ ) and field ( $\xi_{\text{OH},E}$ ) are approximately  $\xi_{\text{OH},j}^{\text{Nb}} \approx 0.025$  ( $\xi_{\text{OH},E}^{\text{Nb}} \approx \frac{\hbar}{2e} 6.1 \times 10^4 (\Omega \text{ m})^{-1}$ ) and  $\xi_{\text{OH},j}^{\text{Ru}} \approx 0.016$  [ $\xi_{\text{OH},E}^{\text{Ru}} \approx \frac{\hbar}{2e} 5.86 \times 10^4 (\Omega \text{ m})^{-1}$ ] for Nb and Ru, respectively. From this fit, we calculate  $\lambda_{\text{Ni}}$  of Ni is



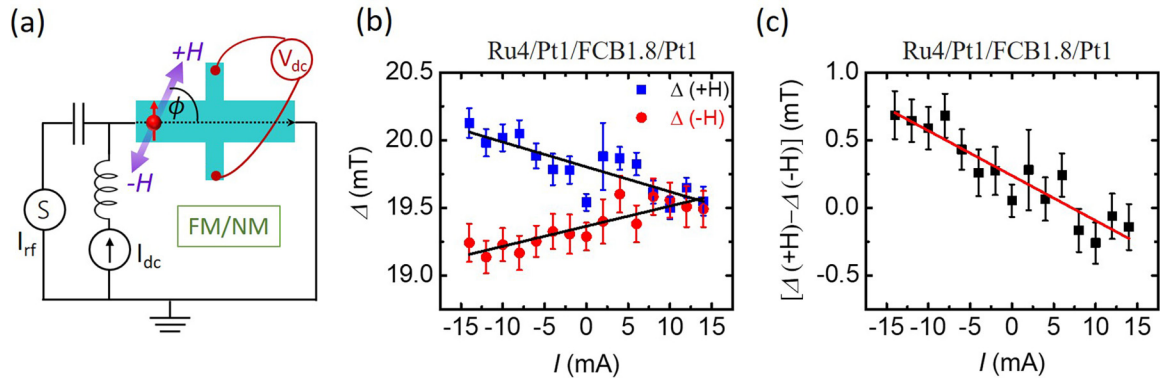


FIG. 5. (a) Schematic representation of dc-bias STFMR setup. (b) Measured linewidth ( $\Delta$ ) as a function of applied dc current ( $I$ ) for positive and negative field sweeps. (c) The difference in the linewidth [ $\Delta(+H) - \Delta(-H)$ ] for the positive and negative swept field as a function of applied dc bias current.

$2.2 \pm 0.7$  nm and  $2.7 \pm 0.9$  nm in Nb/Ni and Ru/Ni samples, respectively, suggesting that 8–10 nm Ni is needed to obtain the full strength of OHT from  $J_{\text{OH} \rightarrow \text{S}}$  (Fig. 2). This length scale is substantially larger than the regular SHT [28,29] and this could possibly be a key signature of OHT uniquely different from the SHT. The inset of Fig. 2 shows plots of  $1/\xi_{\text{FMR}}$  vs  $1/t_{\text{Ni}}$  which has been a standard way to quantify the  $\xi_{\text{DL}}$  using the STFMR measurements in the presence of the interfacial FLT [39]. Using this technique, we find that  $\xi_{\text{DL}}$  approaches infinity for Nb/Ni, which is not realistic, highlighting the importance of the proposed alternate expression for the torque [Eq. (1)]. Note that in this analysis, we consider only the DLT produced by the effective spin current [Eq. (1)] and neglect interfacial opFLT from the spin current as it is generally small [41]. However, the proposed model [Eq. (1)] can fairly explain the thickness dependence of the measured torques (Fig. 3). We find that the AMR of Ni-based films is very large (more than 1%, largest among Py, Co, Fe, and FeCoB) that enhances the rectified dc voltage from the spin torques where spin-pumping effects would be negligible [44].

### C. Harnessing orbital current to spin current using the SOC of Pt

In this section we show the conversion of  $J_{\text{OH} \rightarrow \text{S}}$  using the SOC of a HM (Pt in this case) that can produce a torque on any FM for broader technological application. We implement devices as shown in Fig. 1(c) with Ru being the source of  $J_{\text{OH}}$  and Pt being the converter of  $J_{\text{OH} \rightarrow \text{S}}$ . Even though Ru exhibits a negligible SHE [Fig. 2(c)] ( $\xi_{\text{DL},J} \approx +0.001$ ), a sizable DLT is observed in Ru/Pt(1)/FCB/Pt(1) heterostructures,  $\xi_{\text{DL},J} = 0.03 \pm 0.004$  for a Ru thickness 4 nm [Fig. 4(a)] and  $\xi_{\text{DL},J} = 0.029 \pm 0.004$  for a Ru thickness 2 nm [Fig. 4(b)], suggesting the  $J_{\text{OH}}$  generation in the bulk of Ru by OHE. In this method the sign of DLT (hence  $V_S$ ) should have the same sign of SHE of Pt since  $J_{\text{OH}}$  is positive in these metals [4,10] which is also evident in Ru(4)/Pt(1)/FCB/Pt(1) samples [Figs. 4(a) and 4(b)]. Note that  $J_{\text{SH}}$  generated by 1 nm Pt nearly cancels from both sides producing negligible torques in

Ru/Pt/FCB/Ru samples (see the Supplemental Material [31]). Further, we have quantified the  $\xi_{\text{DL},E}$  as a function of Pt thickness,  $t_{\text{Pt}}$  [Fig. 4(c)], which shows the enhancement of DLT up to  $t_{\text{Pt}} = 1$  nm and then an exponential decay of the DLT with the approximate estimated decay length of 2.5 nm. This behavior suggests that conversion of  $J_{\text{OH} \rightarrow \text{S}}$  in the Pt takes place at a much shorter length scale ( $< 1$  nm) as compared to Ni (Fig. 3). For the Nb/Pt(1)/Py/Pt(1) samples we also observe a large enhancement of  $V_S$  but with the opposite sign [Figs. 4(d) and 4(e)] which cannot be explained by the OHE. We speculate this could be due to the interface generated spin [46–48] and/or orbital current [15,49]. While this is an interesting finding in itself, but not the main focus of this work, we provide more discussions in the Supplemental Material [31].

### D. Measurement of dc-bias STFMR

As an independent measurement, we have performed the linewidth ( $\Delta$ ) analysis as a function of applied dc-bias current in Ru(4)/Pt(1)/FeCoB(1.8)/Pt(1) samples in the planar Hall geometry, which is an improved dc-bias STFMR technique [50], capable of measuring the dampinglike torque more sensitively. In this technique, both rf current and dc current are simultaneously applied in the longitudinal direction using a bias tee as shown in Fig. 5(a) while a transverse dc voltage is measured by sweeping the external magnetic field ( $H$ ) at angles  $\phi = 65^\circ$  and  $-115^\circ$  with respect to the current flow direction ( $\phi = 65^\circ$  corresponds to  $+H$  sweep and  $\phi = -115^\circ$  corresponds to  $-H$  sweep). The transverse voltage reduces the background offset voltage and hence improves the signal to noise ratio as discussed in Ref. [50]. FeCoB of 1.8 nm thickness is used in this study as it is in-plane magnetized and, due to the lower thickness, it enables us to measure a greater change in the linewidth. Figure 5(b) clearly shows a linear trend of the linewidth modulation as a function of applied dc-bias current with opposite signs of the slope for  $+H$  and  $-H$  sweeps. Figure 5(c) shows the difference of linewidth for  $+H$  and  $-H$  sweeps as a function of the applied dc-bias current that eliminates any contribution from the heating signal which can be appreciated by the linear modulation of the

TABLE I. The efficiencies of DLT per unit current density ( $\xi_{DL,J}$ ) and per unit electric field ( $\xi_{DL,E}$ ) for different samples suggesting a negligible SHT in Nb (or Ru)/FeCoB samples, sizable DLT (SHT combined with OHT) in Nb (or Ru)/Ni samples (including the sign change in Nb), and large DLT in Ru/Pt/FeCoB/Pt samples driven by  $J_{OH}$ .

Net DLT	Nb/FeCoB	Ru/FeCoB	Nb/Ni	Ru/Ni	Ru/Pt/FeCoB/Pt
$\xi_{DL,J}$	$-0.001 \pm 0.001$	$+0.001 \pm 0.001$	$+0.018 \pm 0.005$	$+0.019 \pm 0.005$	$+0.03 \pm 0.004$
$\xi_{DL,E} 10^3 \frac{\hbar}{2e} (\Omega \text{ m})^{-1}$	$-2.4 \pm 2.4$	$+3.6 \pm 3.6$	$+44 \pm 12$	$+69.6 \pm 18.3$	$+110 \pm 15$

linewidth difference  $[\Delta(+H) - \Delta(-H)]$  with the applied dc-bias current. From these measurements we can independently quantify the dampinglike torque efficiency to be  $\xi_{DL,E} = \frac{\hbar}{2e} (7.8 \pm 2.0) \times 10^4 (\Omega \text{ m})^{-1}$  which is quite comparable to the previously obtained values on the Ru(4)/Pt(1)/FCB(5)/Pt(1) samples [ $\xi_{DL,E} = \frac{\hbar}{2e} (11.0 \pm 1.5) \times 10^4 (\Omega \text{ m})^{-1}$ ] as summarized in Table I.

## VI. CONCLUSION

In summary, we report the generation of a large orbital-Hall current by elemental Ru and Nb determining the lower bound of the OHC to be  $\frac{\hbar}{2e} (6.1 \pm 1, 5) \times 10^4 (\Omega \text{ m})^{-1}$  and  $\frac{\hbar}{2e} (5.86 \pm 1.4) \times 10^4 (\Omega \text{ m})^{-1}$ , respectively, which is an order of magnitude larger than the measured SHC, providing direct agreement with the theoretical predictions which was not possible to ascertain from the previous measurements done on the oxide-based nonmagnetic films due to the poorly defined structure. We report two striking observations, i.e., (1) strong dependence of the OHT on the adjacent ferromagnet (including the sign reversal in some cases such as Nb/Ni) and (2) the long-range action of the torques that tend to saturate for a Ni thickness approximately 8–10 nm. Both these observations cannot be explained by the regular spin-Hall effect induced spin-orbit (spin-Hall torque) torque and these could be key signatures of the orbital-Hall torque. We finally unambiguously demonstrate that an additional HM layer can generate an efficient torque by converting  $J_{OH}$  to  $J_S$  providing the necessary flexibility for the device applications.

*Note added.* During the preparation of the paper we became aware of a recent and relevant work of orbital-torques generated by Ti [27].

## ACKNOWLEDGMENTS

D.G. and Y.M. thank the Jülich Supercomputing Centre for providing computational resources under Project No. jiff40. This work was funded by the Deutsche Forschungsgemeinschaft (DFG). A.B., F.K., R.G., G.J., and M.K. thank the Graduate School of Excellence Materials Science in Mainz (MAINZ, GSC266); Spin+X (A01, A11, B02) TRR 173-268565370 and Project No. 358671374; the Horizon 2020 Framework Programme of the European Commission under FETOpen Grant Agreement No. 863155 (s-Nebula); the European Research Council Grant Agreement No. 856538 (3D MAGiC); and the Research Council of Norway through its Centers of Excellence funding scheme, Project No. 262633 “QuSpin.” A.B. thanks the Alexander von Humboldt foundation for support through the postdoctoral fellowship.

The sample growth, device fabrication, device characterization and data analysis were primarily carried out by A.B. The theoretical calculations were done by D.G. under the supervision of Y.M. F.K. helped in the thin-film deposition under the supervision of G.J. R.G. carried out dc-bias STFM. A.B. and M.K. wrote the paper with input from other coauthors. M.K. has been the principal investigator and supervised the whole project.

- 
- [1] A. Manchon, J. Železný, I. M. Miron, T. Jungwirth, J. Sinova, A. Thiaville, K. Garello, and P. Gambardella, Current-induced spin-orbit torques in ferromagnetic and antiferromagnetic systems, *Rev. Mod. Phys.* **91**, 035004 (2019).
  - [2] B. Dieny, I. L. Prejbeanu, K. Garello, P. Gambardella, P. Freitas, R. Lehndorff, W. Raberg, U. Ebels, S. O. Demokritov, J. Akerman, A. Deac, P. Pirro, C. Adelmann, A. Anane, A. V. Chumak, A. Hirohata, S. Mangin, S. O. Valenzuela, M. C. Onbaşlı, M. D’Aquino *et al.*, Opportunities and challenges for spintronics in the microelectronics industry, *Nat. Electron.* **3**, 446 (2020).
  - [3] J. Sinova, S. O. Valenzuela, J. Wunderlich, C. H. Back, and T. Jungwirth, Spin Hall effects, *Rev. Mod. Phys.* **87**, 1213 (2015).
  - [4] T. Tanaka, H. Kontani, M. Naito, T. Naito, D. S. Hirashima, K. Yamada, and J. Inoue, Intrinsic spin Hall effect and orbital Hall effect in 4d and 5d transition metals, *Phys. Rev. B* **77**, 165117 (2008).
  - [5] D. Go, D. Jo, C. Kim, and H. Lee, Intrinsic Spin and Orbital Hall Effects from Orbital Texture, *Phys. Rev. Lett.* **121**, 086602 (2018).
  - [6] D. Jo, D. Go, and H.-W. Lee, Gigantic intrinsic orbital Hall effects in weakly spin-orbit coupled metals, *Phys. Rev. B* **98**, 214405 (2018).
  - [7] D. Go and H.-W. Lee, Orbital torque: Torque generation by orbital current injection, *Phys. Rev. Res.* **2**, 013177 (2020).
  - [8] D. Go, F. Freimuth, J.-P. Hanke, F. Xue, O. Gomonay, K.-J. Lee, S. Blügel, P. M. Haney, H.-W. Lee, and Y. Mokrousov, Theory of current-induced angular momentum transfer dynamics in spin-orbit coupled systems, *Phys. Rev. Res.* **2**, 033401 (2020).
  - [9] D. Go, D. Jo, K.-W. Kim, S. Lee, M.-G. Kang, B.-G. Park, S. Blügel, H.-W. Lee, and Y. Mokrousov, Long-range orbital magnetoelectric torque in ferromagnets, [arXiv:2106.07928](https://arxiv.org/abs/2106.07928).

- [10] L. Salemi and P. M. Oppeneer, First-principles theory of intrinsic spin and orbital Hall and Nernst effects in metallic monoatomic crystals, *Phys. Rev. Mater.* **6**, 095001 (2022).
- [11] S. Bhowal and S. Satpathy, Intrinsic orbital moment and prediction of a large orbital Hall effect in two-dimensional transition metal dichalcogenides, *Phys. Rev. B* **101**, 121112 (2020).
- [12] L. M. Canonico, T. P. Cysne, A. Molina-Sanchez, R. B. Muniz, and T. G. Rappoport, Orbital Hall insulating phase in transition metal dichalcogenide monolayers, *Phys. Rev. B* **101**, 161409 (2020).
- [13] A. Pezo, D. García Ovalle, and A. Manchon, Orbital Hall effect in crystals: Interatomic versus intra-atomic contributions, *Phys. Rev. B* **106**, 104414 (2022).
- [14] D. Go, D. Jo, H.-W. Lee, M. Kläui, and Y. Mokrousov, Orbitronics: Orbital currents in solids, *EPL* **135**, 37001 (2021).
- [15] S. Ding, A. Ross, D. Go, L. Baldrati, Z. Ren, F. Freimuth, S. Becker, F. Kammerbauer, J. Yang, G. Jakob, Y. Mokrousov, and M. Kläui, Harnessing Orbital-to-Spin Conversion of Interfacial Orbital Currents for Efficient Spin-Orbit Torques, *Phys. Rev. Lett.* **125**, 177201 (2020).
- [16] H. An, Y. Kageyama, Y. Kanno, N. Enishi, and K. Ando, Spin-torque generator engineered by natural oxidation of Cu, *Nat. Commun.* **7**, 13069 (2016).
- [17] T. Gao, A. Qaiumzadeh, H. An, A. Musha, Y. Kageyama, J. Shi, and K. Ando, Intrinsic Spin-Orbit Torque Arising from the Berry Curvature in a Metallic-Magnet/Cu-Oxide Interface, *Phys. Rev. Lett.* **121**, 017202 (2018).
- [18] J. Kim, D. Go, H. Tsai, D. Jo, K. Kondou, H.-W. Lee, and Y. Otani, Nontrivial torque generation by orbital angular momentum injection in ferromagnetic-metal/Cu/Al<sub>2</sub>O<sub>3</sub> trilayers, *Phys. Rev. B* **103**, L020407 (2021).
- [19] L. Liao, F. Xue, L. Han, J. Kim, R. Zhang, L. Li, J. Liu, X. Kou, C. Song, F. Pan, and Y. Otani, Efficient orbital torque in polycrystalline ferromagnetic/Ru/Al<sub>2</sub>O<sub>3</sub>: Theory and experiment, *Phys. Rev. B* **105**, 104434 (2022).
- [20] K. Ueda, C. F. Pai, A. J. Tan, M. Mann, and G. S. D. Beach, Effect of rare earth metal on the spin-orbit torque in magnetic heterostructures, *Appl. Phys. Lett.* **108**, 232405 (2016).
- [21] A. Bose, H. Singh, V. K. Kushwaha, S. Bhuktare, S. Dutta, and A. A. Tulapurkar, Sign Reversal of Fieldlike Spin-Orbit Torque in an Ultrathin Cr/Ni Bilayer, *Phys. Rev. Appl.* **9**, 014022 (2018).
- [22] A. Bose, J. N. Nelson, X. S. Zhang, P. Jadaun, R. Jain, D. G. Schlom, D. C. Ralph, D. A. Muller, K. M. Shen, and R. A. Buhrman, Effects of anisotropic strain on spin-orbit torque produced by the Dirac nodal line semimetal IrO<sub>2</sub>, *ACS Appl. Mater. Interfaces* **12**, 55411 (2020).
- [23] D. Lee, D. Go, H.-J. Park, W. Jeong, H.-W. Ko, D. Yun, D. Jo, S. Lee, G. Go, J. H. Oh, K.-J. Kim, B.-G. Park, B.-C. Min, H. C. Koo, H.-W. Lee, O. Lee, and K.-J. Lee, Orbital torque in magnetic bilayers, *Nat. Commun.* **12**, 6710 (2021).
- [24] G. Sala and P. Gambardella, Giant orbital Hall effect and orbital-to-spin conversion in 3d, 5d, and 4f metallic heterostructures, *Phys. Rev. Res.* **4**, 033037 (2022).
- [25] S. Lee, M.-G. Kang, D. Go, D. Kim, J.-H. Kang, T. Lee, G.-H. Lee, J. Kang, N. J. Lee, Y. Mokrousov, S. Kim, K.-J. Kim, K.-J. Lee, and B.-G. Park, Efficient conversion of orbital Hall current to spin current for spin-orbit torque switching, *Commun. Phys.* **4**, 234 (2021).
- [26] S. Dutta and A. A. Tulapurkar, Observation of nonlocal orbital transport and sign reversal of dampinglike torque in Nb/Ni and Ta/Ni bilayers, *Phys. Rev. B* **106**, 184406 (2022).
- [27] H. Hayashi, D. Jo, D. Go, T. Gao, S. Haku, Y. Mokrousov, H.-W. Lee, and K. Ando, Observation of long-range orbital transport and giant orbital torque, *Commun. Phys.* **6**, 32 (2023).
- [28] D. C. Ralph and M. D. Stiles, Spin transfer torques, *J. Magn. Magn. Mater.* **320**, 1190 (2008).
- [29] A. Brataas, A. D. Kent, and H. Ohno, Current-induced torques in magnetic materials, *Nat. Mater.* **11**, 372 (2012).
- [30] Y. Choi, D. Jo, K. Ko, D. Go, and H. Lee, Observation of the orbital Hall effect in a light metal Ti, [arXiv:2109.14847v1](https://arxiv.org/abs/2109.14847v1).
- [31] See Supplemental Material at <http://link.aps.org/supplemental/10.1103/PhysRevB.107.134423> for the details of sample preparation, magnetometry data, and DFT calculation.
- [32] <https://www.flapw.de>.
- [33] E. Wimmer, H. Krakauer, M. Weinert, and A. J. Freeman, Full-potential self-consistent linearized-augmented-plane-wave method for calculating the electronic structure of molecules and surfaces: O<sub>2</sub> molecule, *Phys. Rev. B* **24**, 864 (1981).
- [34] J. P. Perdew, K. Burke, and M. Ernzerhof, Generalized Gradient Approximation Made Simple, *Phys. Rev. Lett.* **77**, 3865 (1996).
- [35] G. Pizzi, V. Vitale, R. Arita, S. Blügel, F. Freimuth, G. Géranton, M. Gibertini, D. Gresch, C. Johnson, T. Koretsune, J. Ibañez-Azpiroz, H. Lee, J.-M. Lihm, D. Marchand, A. Marrazzo, Y. Mokrousov, J. I. Mustafa, Y. Nohara, Y. Nomura, L. Paulatto *et al.*, WANNIER90 as a community code: New features and applications, *J. Phys.: Condens. Matter* **32**, 165902 (2020).
- [36] F. Freimuth, Y. Mokrousov, D. Wortmann, S. Heinze, and S. Blügel, Maximally localized Wannier functions within the FLAPW formalism, *Phys. Rev. B* **78**, 035120 (2008).
- [37] L. Liu, T. Moriyama, D. C. Ralph, and R. A. Buhrman, Spin-Torque Ferromagnetic Resonance Induced by the Spin Hall Effect, *Phys. Rev. Lett.* **106**, 036601 (2011).
- [38] D. Fang, H. Kurebayashi, J. Wunderlich, K. Výborný, L. P. Zárbo, R. P. Campion, A. Casiraghi, B. L. Gallagher, T. Jungwirth, and A. J. Ferguson, Spin-orbit-driven ferromagnetic resonance, *Nat. Nanotechnol.* **6**, 413 (2011).
- [39] C.-F. Pai, Y. Ou, L. H. Vilela-Leão, D. C. Ralph, and R. A. Buhrman, Dependence of the efficiency of spin Hall torque on the transparency of Pt/ferromagnetic layer interfaces, *Phys. Rev. B* **92**, 064426 (2015).
- [40] A. Bose, N. J. Schreiber, R. Jain, D.-F. Shao, H. P. Nair, J. Sun, X. S. Zhang, D. A. Muller, E. Y. Tsymlal, D. G. Schlom, and D. C. Ralph, Tilted spin current generated by the collinear antiferromagnet ruthenium dioxide, *Nat. Electron.* **5**, 267 (2022).
- [41] Y.-T. Chen, S. Takahashi, H. Nakayama, M. Althammer, S. T. B. Goennenwein, E. Saitoh, and G. E. W. Bauer, Theory of spin Hall magnetoresistance, *Phys. Rev. B* **87**, 144411 (2013).
- [42] C.-F. Pai, L. Liu, Y. Li, H. W. Tseng, D. C. Ralph, and R. A. Buhrman, Spin transfer torque devices utilizing the giant spin Hall effect of tungsten, *Appl. Phys. Lett.* **101**, 122404 (2012).
- [43] A. Bose, R. Jain, J. J. Bauer, R. A. Buhrman, C. A. Ross, and D. C. Ralph, Origin of transverse voltages generated by thermal gradients and electric fields in ferrimagnetic-insulator/heavy-metal bilayers, *Phys. Rev. B* **105**, L100408 (2022).
- [44] S. Karimeddiny, J. A. Mittelstaedt, R. A. Buhrman, and D. C. Ralph, Transverse and Longitudinal Spin-Torque Ferro-

- magnetic Resonance for Improved Measurement of Spin-Orbit Torque, [Phys. Rev. Appl.](#) **14**, 024024 (2020).
- [45] H. Wang, C. Du, P. Chris Hammel, and F. Yang, Spin current and inverse spin Hall effect in ferromagnetic metals probed by  $\text{Y}_3\text{Fe}_5\text{O}_{12}$ -based spin pumping, [Appl. Phys. Lett.](#) **104**, 202405 (2014).
- [46] V. P. Amin, J. Zemen, and M. D. Stiles, Interface-Generated Spin Currents, [Phys. Rev. Lett.](#) **121**, 136805 (2018).
- [47] A. Manchon, H. C. Koo, J. Nitta, S. M. Frolov, and R. A. Duine, New perspectives for Rashba spin-orbit coupling, [Nat. Mater.](#) **14**, 871 (2015).
- [48] S. Dutta, A. Bose, A. A. Tulapurkar, R. A. Buhrman, and D. C. Ralph, Interfacial and bulk spin Hall contributions to field-like spin-orbit torque generated by iridium, [Phys. Rev. B](#) **103**, 184416 (2021).
- [49] D. Go, D. Jo, T. Gao, K. Ando, S. Blügel, H.-W. Lee, and Y. Mokrousov, Orbital Rashba effect in a surface-oxidized Cu film, [Phys. Rev. B](#) **103**, L121113 (2021).
- [50] A. Bose, S. Dutta, S. Bhuktare, H. Singh, and A. A. Tulapurkar, Sensitive measurement of spin-orbit torque driven ferromagnetic resonance detected by planar Hall geometry, [Appl. Phys. Lett.](#) **111**, 162405 (2017).